Effect of Fiber Rupture on Tensile Properties of Short Fiber Composites

Mohamed Maalej,[1] Victor C. Li,[2] Members, ASCE, and Toshiyuki Hashida[3]

Abstract: A probabilistic-based micromechanical model has been developed for the postcracking behavior of a brittle matrix reinforced with short, randomly distributed fibers. The model that predicts the composite-bridging stress crack-opening displacement (COD) relationship, accounts for fiber pullout, fiber tensile rupture, and a local frictional effect called snubbing. However, it does not account for fiber bending rupture, and the possible effect of matrix spalling at the exit points of inclined fibers from the matrix. The model assumes a fiber/matrix interface that is controlled by a constant frictional bond stress. The model is used to predict the composite tensile strength and fracture energy. Comparisons of model-predicted bridging stress-COD relationship with experimental data, where fiber rupture has occurred, show reasonable agreement supporting the validity of the proposed model. The model is then used to perform a parametric study to evaluate the effect of the micromechanical parameters on the composite tensile strength and fracture energy. The study suggests that this model can be used to design the composite for optimum performance.

INTRODUCTION

The problems of cracking and low toughness that brittle materials show may be overcome by the addition of short, randomly distributed fibers. The main advantages of adding fibers to a brittle matrix can be summarized as (1) significant increase in toughness or energy absorption capacity; (2) possible increase of ultimate tensile strength and/or strain; and (3) good crack-width control mechanism. These desirable characteristics have usually been achieved at relatively low fiber-volume fractions (less than 5%). However, these advantages are generally associated with an increase in the overall cost of the materials, mainly due to the added cost of fibers and further material processing. To use the minimum amount of fibers and achieve maximum performance improvement, researchers have been developing analytical tools to optimize the design of these fiber composites.

The postcracking behavior of discontinuous random fiber-reinforced brittle-matrix composites (DRFRC) can be predicted by the use of a composite bridging stress-COD (σ_c-δ) relationship. The latter describes the constitutive relationship between the traction acting across a matrix crack plane and the separation distance of the crack faces (i.e., COD) in a singly precracked uniaxial tensile specimen loaded quasi-statically to complete failure (Li et al. 1987). The σ_c-δ relationship is a fundamental material property that contains information regarding the composite postcracking strength and fracture energy. The σ_c-δ curve consists of an ascending branch called the prepeak σ_c-δ curve and a descending branch called the postpeak σ_c-δ curve (or the tension-softening curve). The prepeak σ_c-δ relationship is one of the important material properties that govern the composite first cracking strength and the presence or absence of multiple cracking in the composite (Li and Leung 1992). In a strain-hardening composite, where a series of parallel cracks develop in a specimen prior to reaching the peak load [e.g., Krenchel and Hansen (1992) and Li and Wu (1992)], the prepeak (postcracking) behavior can be characterized by a stress-strain curve. The peak of this curve must coincide with that of the prepeak σ_c-δ curve. Therefore, for strain-hardening materials, the tensile strength can be predicted by computing the peak of the prepeak σ_c-δ curve. Furthermore, the postpeak composite behavior can be predicted by computing the postpeak σ_c-δ curve. For quasi-brittle materials, where failure occurs by the development of a single crack, the postcracking behavior can only be described by a stress-displacement curve. This curve may or may not include a portion of the prepeak σ_c-δ curve depending on the COD in the middle of the specimen at the time the first crack spreads through the specimen cross section [more details can be found in Li and Leung (1992)]. For both materials, the composite-bridging fracture energy can be predicted by integrating the area under the σ_c-δ curve.

Assuming a purely frictional fiber/matrix interface and complete fiber pullout, Visalvanich and Naaman (1983) derived a semiempirical model for the tension-softening curve in discontinuous randomly distributed steel fiber-reinforced mortar. With the same assumptions, Li (1992) derived an analytic model [the fiber pullout model (FPM)] that predicts the complete σ_c-δ curve for DRFRC, taking into account an additional frictional effect called the snubbing effect. The model provided a good prediction for the postcracking strength, the tension-softening curve, and composite fracture energy for a number of composites in which the fibers did not rupture. However, discrepancies were observed between the prediction of this model and some experimental measurements, which suggests the occurrence of fiber rupture (Li and Wu 1992). Fiber rupture has also been experimentally observed in carbon, glass, polypropylene, stainless steel, and SiC DRFRC. Li et al. (1991) studied the fracture energy associated with fiber bridging in DRFRC taking into account the effect of fiber tensile rupture.

This paper extends the fiber pullout model by explicitly accounting for potential fiber tensile rupture. However, the new model [referred to as the fiber pullout and rupture model (FPRM)] does not account for fiber bending rupture and the possible effect of matrix spalling at the exit points of inclined fibers from the matrix. Moreover, the model does not account for the possible interaction between neighboring fibers, and the modification of the relevant matrix properties (e.g., modulus and packing density) by the addition of fibers, because these may introduce additional voids in the matrix. These voids may also affect the fiber/matrix interfacial bond strength. Preliminary experimental results suggest that the bond strength deteriorates with increasing the fiber-volume fraction. For this reason, it is necessary to tailor the microproperties (fiber,

[1]Res. Fellow, ACE-MRL, Dept. of Civ. and Envir. Engrg., Univ. of Michigan, Ann Arbor, MI 48109-2125.

[2]Prof., ACE-MRL, Dept. of Civ. and Envir. Engrg., Univ. of Michigan, Ann Arbor, MI.

[3]Assoc. Prof., Res. Inst. for Fracture Technol., Tohoku Univ., Sendai 980, Japan.

Note. Associate Editor: Jean-Lou A. Chameau. Discussion open until January 1, 1996. To extend the closing date one month, a written request must be filed with the ASCE Manager of Journals. The manuscript for this paper was submitted for review and possible publication on April 5, 1993. This paper is part of the ***Journal of Engineering Mechanics***, Vol. 121, No. 8, August, 1995. ©ASCE, ISSN 0733-9399/95/0008-0903–0913/ $2.00 + $.25 per page. Paper No. 5941.

matrix, and interface properties), such as targeted material properties (e.g., tensile strength and fracture energy), which can be achieved by the use of a minimum fiber-volume fraction. In this case, the interaction between neighboring fibers and the modification of the matrix properties by the presence of fibers can be significantly reduced.

After experimental validation, the FPRM is then used to perform a parametric study that evaluates the effect of each micromechanical parameter on the composite tensile strength and fracture energy. The results of the parametric study suggest that the model can be used to optimize the design of DRFRC in terms of composite tensile strength and fracture energy.

SINGLE-FIBER STRESS-DISPLACEMENT RELATIONSHIP

In this paper we adopt a simple model of fiber/matrix interface debonding based on a purely frictional strength. In this model the elastic bond is ignored; therefore, what we refer to as debonding is the activation of the frictional slip zone. This activation is assumed to take place at the moment the fiber is loaded. The validity of this friction-controlled interface, used in most studies of cement-based fiber composites, has recently been experimentally confirmed by Li and Chan (1994), at least for steel and brass fibers in a cement matrix. Consider a single fiber with diameter d_f, length L_f, elastic modulus E_f, tensile strength σ_{fu}, and an interfacial frictional bond strength τ. The fiber is bridging a matrix plane crack as shown in Fig. 1. The elastic modulus of the matrix is E_m and the fiber volume fraction is V_f. During frictional debonding, the fiber debonding stress σ_d versus displacement δ is given by the following relationship (Li and Leung 1992):

$$\sigma_d = [4(1 + \eta)\tau E_f(\delta/d_f)]^{1/2}$$

$$= (4\sigma_o/V_f)[\hat{\delta}/\hat{\delta}^*]^{1/2}, \quad \text{for} \quad \delta \le \delta_o \tag{1}$$

where $\eta = V_f(E_f/E_m)/(1 - V_f)$; $\sigma_o = V_f\tau L_f/(2d_f)$; $\delta = \delta/(L_f/2)$; $\delta_o = 4l(\tau/E_f)(l/d_f)/(1 + \eta)$; and $\hat{\delta}^* = 2(\tau/E_f)(L_f/d_f)/(1 + \eta)$. In (1), δ_o = fiber displacement at which frictional debonding has reached the end of the embedment length l, assuming fiber rupture has not occurred. After this stage, fiber pullout proceeds. The pullout stress-displacement relationship is approximated by the following equation (Li 1992):

$$\sigma_p = (4\tau/d_f)[l - \delta + \delta_o]$$

$$= (4\sigma_o/V_f)[\hat{l} + \hat{\delta}^*\hat{l}^2 - \hat{\delta}], \quad \text{for} \quad \delta_o \le \delta \le l \tag{2}$$

where $\hat{l} = l/(L_f/2)$. The preceding two equations hold true for fibers loaded in a direction along their axis. Randomly distributed fibers, however, generally do not lie in a direction normal to the matrix-crack plane. The misalignment between fiber axis and crack plane normal results in a local frictional effect called snubbing (Li 1992), which can be incorporated into the debonding and pullout stresses as follows [Fig. 2(a)]:

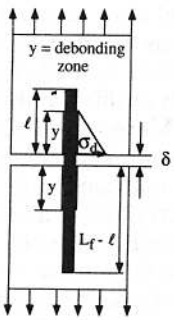

FIG. 1. Single Fiber Bridging Plane Crack

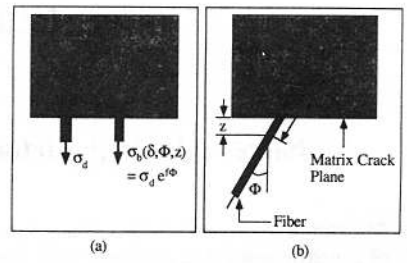

FIG. 2. Fiber Orientation and Snubbing Effect

$$\sigma_b(\delta, \Phi, z) = \sigma_d e^{f\Phi}, \quad \text{for} \quad \delta \le \delta_o \tag{3a}$$

$$\sigma_b(\delta, \Phi, z) = \sigma_p e^{f\Phi}, \quad \text{for} \quad \delta_o \le \delta \le l \tag{3b}$$

where f = an interface material parameter called the snubbing friction coefficient. Typical values of f range between 0 and 1. The snubbing coefficient f can be determined for a particular fiber matrix interface by conducting a series of single fiber pullout tests at different angles ranging between 0° and 90°, then plotting the maximum load P_{max} versus the angle Φ and fitting this curve to an equation of the form $P_{max} = P_{max}(\Phi = 0)e^{f\Phi}$, where f = fitting parameter. For instance, such an experiment led to f values of 0.99 and 0.70 for nylon and polypropylene fibers embedded in a normal-strength mortar matrix (Li et al. 1990). The fiber centroidal location z and orientation Φ are defined in Fig. 2(b). The embedment length l can be expressed in terms of the fiber length L_f, fiber centroidal location z, and fiber orientation Φ as follows:

$$l = (L_f/2) - (z/\cos\Phi) \tag{4}$$

In (1)–(3), it was assumed that the stress in the loaded fiber never reaches its tensile strength σ_{fu}. However, it is reasonable to assume that for certain fiber/matrix systems, the combination of fiber embedment length, diameter, inclined angle and interfacial and snubbing friction may lead to stresses in a number of loaded fibers exceeding their tensile strength. In this case, those fibers are expected to break.

Consider now a fiber/matrix composite in which potential fiber rupture can occur. It is assumed that all fibers are identical and have uniform tensile strength along their length. In this case, when fiber rupture occurs, it would be at the matrix-crack plane. Therefore, when a fiber breaks, it no longer contributes to the composite bridging stress.

The critical embedment length l_u, beyond which potential fiber rupture can occur, is determined by setting the fiber bridging stress $\sigma_b(\delta_o, \Phi, z)$ equal to σ_{fu}. It follows that

$$l_u = L_c e^{-f\Phi} \tag{5}$$

where $L_c = \sigma_{fu}d_f/(4\tau)$. If the snubbing effect was not considered ($f = 0$), fibers would rupture if their embedment length l is greater than L_c. Therefore, all fibers having an embedment length in the range $[L_c, L_f/2]$ would rupture rather than pull out. However, due to the snubbing effect, (5) shows that all fibers for which the embedment length and orientation belong to a two-dimensional space $\{l \in [0, L_f/2]$ and $\Phi \in [0, \pi/2]$ such that $l \ge L_c e^{-f\Phi}\}$ rupture rather than pull out. Based on its definition, this two-dimensional space (referred to as fiber-rupture space) is also equal to the following:

$$S = \{l \in [L_c e^{-f\pi/2}, L_f/2] \quad \text{and} \quad \Phi \in [0, \pi/2]$$

$$\text{such that} \quad l \ge L_c e^{-f\Phi}\} \tag{6}$$

Consequently, there exists a minimum critical fiber length L_r equal to $2L_c e^{-f\pi/2}$ beyond which fiber rupture starts to occur. Therefore, if the fiber length is less than L_r, the fiber-rupture space S would be empty [Fig. 3(a)] and all fibers would pull out subsequent to complete debonding. If, on the other hand,

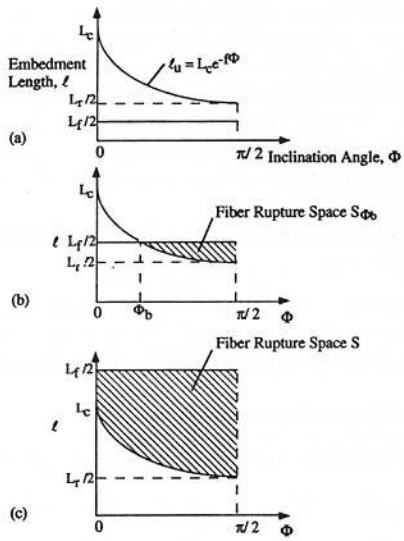

FIG. 3. Fiber Rupture Space

L_f is greater than L_r, the fiber-rupture space would be nonempty and fiber rupture is expected. In the particular case when the fiber length is greater than L_r but less than $2L_c$ (critical fiber length), the fiber rupture space would be equal to [Fig. 3(b)] the following:

$$S_{\Phi b} = \{l \in [L_c e^{-f\pi/2}, L_f/2] \quad \text{and} \quad \Phi \in [\Phi_b, \pi/2] \quad \text{such that} \quad l \geq L_c e^{-f\Phi}\} \tag{7}$$

where

$$\Phi_b = -(1/f)\ln(L_f/2L_c) \tag{8}$$

Note in this case that all fibers oriented at an angle less than Φ_b (i.e., $0 \leq \Phi \leq \Phi_b$) pull out subsequent to complete debonding. When the fiber length is greater than $2L_c$, rupture can occur for any fiber orientation, provided the embedment length is greater than the critical embedment length l_u [Fig. 3(c)]. When the fiber-rupture space is nonempty, fibers with an embedment length l and orientation Φ, which belong to S, rupture after incomplete debonding. All other fibers are pulled out subsequent to complete debonding.

Fig. 3 shows that fibers at 90° could either rupture or pull out depending on their embedment length. However, in reality, a fiber that is oriented at exactly 90° may not be contributing at all to the composite bridging stress as it will be lying tangent to the matrix-crack plane. Because only a small fraction of the bridging fibers should be oriented at 90°, and for simplicity, the model assumes that fibers oriented at 90° are contributing fibers.

If a fiber does rupture, this must occur some time during debonding ($\delta \leq \delta_o$), because the fiber bridging stress always decays during pullout [an exception would be slip hardening during pullout of some polymeric fibers that experience severe abrasion (Li et al. 1990); this case will not be analyzed in this paper]. At the particular moment when a fiber breaks, the COD is at a critical value δ_u, which can be determined by setting the fiber bridging stress $\sigma_b(\delta_u, \Phi, z)$ equal to σ_{fu}. It follows that

$$\delta_u = \delta_c e^{-2f\Phi} \tag{9}$$

where

$$\delta_c = \sigma_{fu}^2 d_f/4(1 + \eta)E_f\tau \tag{10}$$

We can deduce from (9) that fibers oriented at higher inclination angles would rupture before those oriented at lower inclination angles as the matrix crack opens. When the fiber-rupture space is equal to $S_{\Phi b}$ [Fig. 3(b)], fibers oriented at an inclination angle Φ_b are the last ones to rupture. According to (9), those fibers rupture at a COD equal to

$$\delta_c e^{-2f\Phi_b} = \delta_c(L_f/2L_c)^2 = \delta^* \tag{11}$$

Interestingly, this COD corresponds to the stage when debonding is completed for those fibers with the longest embedment length ($l = L_f/2$). Therefore, all surviving fibers will be in a pullout stage as soon as the COD is greater than δ^*. If, on the other hand, the fiber-rupture space is equal to S [Fig. 3(c)], fibers oriented at a zero inclination angle (and having $l \geq l_u$) are the last ones to rupture. According to (9), those fibers rupture at a COD equal to δ_c. Therefore, all surviving fibers will be in a pullout stage as soon as the COD is greater than δ_c.

The fiber bridging stress-displacement relationship for the group of fibers that eventually rupture is defined by a step function, as follows:

$$\sigma_b(\delta, \Phi, z) = \sigma_d U(\delta_c e^{-2f\Phi} - \delta)e^{f\Phi} \tag{12}$$

where

$$U(\delta_c e^{-2f\Phi} - \delta) = 1 \quad \text{for} \quad \delta \leq \delta_c e^{-2f\Phi} \quad \text{or} \quad \Phi \leq \Phi_c \tag{13a}$$

$$U(\delta_c e^{-2f\Phi} - \delta) = 0 \quad \text{for} \quad \delta > \delta_c e^{-2f\Phi} \quad \text{or} \quad \Phi > \Phi_c \tag{13b}$$

$$\text{and} \quad \Phi_c = -(1/2f)\ln(\delta/\delta_c) \tag{14}$$

The parameter Φ_c ($0 \leq \Phi_c \leq \pi/2$), therefore, defines the angle of the fibers that have ruptured at the COD δ.

COMPOSITE BRIDGING STRESS-DISPLACEMENT RELATIONSHIP

Li et al. (1991) showed that the composite bridging stress-COD curve can be approximated by summing the contributions of the individual fibers bridging the matrix-crack plane, according to the following equation:

$$\sigma_c = V_f \int_0^{\pi/2} \int_0^{(L_f/2)\cos\Phi} \sigma_b(\delta, \Phi, z)p(z)p(\Phi)\, dz\, d\Phi \tag{15}$$

where $p(z)$ and $p(\Phi)$ = probability-density functions of the orientation angle and centroidal distance of fibers from the matrix-crack plane. For uniform random distribution they are defined as follows:

$$p(z) = 2/L_f, \quad \text{for} \quad 0 \leq z \leq (L_f/2)\cos\Phi \tag{16}$$

$$p(\Phi) = \sin\Phi, \quad \text{for} \quad 0 \leq \Phi \leq \pi/2 \tag{17}$$

by making the change of variable $x = (2/L_f)(L_f/2 - z/\cos\Phi)$ for z, (15) becomes the following:

$$\sigma_c = (V_f/2) \int_0^{\pi/2} \int_0^1 \sigma_b(\delta, \Phi, x)\sin 2\Phi\, dx\, d\Phi \tag{18}$$

Li (1992) showed that, for the particular case when the fiber length is less than L_r, the composite bridging stress-COD relationship is given by the following:

$$\sigma_c = \sigma_o g[2(\hat{\delta}/\hat{\delta}^*)^{1/2} - (\hat{\delta}/\hat{\delta}^*)], \quad \text{for} \quad \hat{\delta} \leq \hat{\delta}^* \tag{19a}$$

$$\sigma_c = \sigma_o g(1 - \hat{\delta})^2, \quad \text{for} \quad \hat{\delta}^* \leq \hat{\delta} \leq 1 \tag{19b}$$

where

$$g = [2/(4 + f^2)][1 + e^{f\pi/2}] \tag{20}$$

In this paper, the σ_c-δ relationship is extended for the case

in which the fiber length is greater than L_r, and, therefore, fiber rupture is expected.

Prepeak Composite Bridging Stress-Displacement Relationship

The prepeak composite bridging stress-displacement relationship defines the initial portion of the σ_c-δ curve that ends when the fiber-rupture process is completed and all intact fibers are pulling out of the matrix.

$$L_r \le L_f \le 2L_c$$

In this case the fiber-rupture space is equal to $S_{\Phi b}$ [Fig. 3(b)] and all intact fibers are pulling out of the matrix when the COD δ is equal to δ^*. Using (3) and (12) in (18), (21) is obtained (Appendix I)

$$\sigma_c = \sigma_o g[2(\hat{\delta}/\hat{\delta}^*)^{1/2} - (\hat{\delta}/\hat{\delta}^*)], \quad \text{for} \quad \hat{\delta} \le \hat{\delta}_c e^{-f\pi} \tag{21a}$$

$$\sigma_c = \sigma_o\{g(\Phi_c)[2(\hat{\delta}/\hat{\delta}^*)^{1/2} - (\hat{\delta}/\hat{\delta}^*)] + a(-f)\hat{L}_c^2\},$$

$$\text{for} \quad \hat{\delta}_c e^{-f\pi} \le \hat{\delta} \le \hat{\delta}^* \tag{21b}$$

where

$$g(\Phi_c) = [1/(4 + f^2)]\{[f \sin(2\Phi_c) - 2\cos(2\Phi_c)]e^{f\Phi_c} + 2\} \tag{22}$$

$$a(t) = [1/(4 + t^2)]\{[2\cos(2\Phi_c) - t\sin(2\Phi_c)]e^{t\Phi_c} + 2e^{t\pi/2}\} \tag{23}$$

$$L_f \ge 2L_c$$

Here the fiber-rupture space is equal to S [Fig. 3(c)] and all intact fibers are pulling out of the matrix when the COD δ is equal to δ_c. It follows that (Appendix I)

$$\sigma_c = \sigma_o g[2(\hat{\delta}/\hat{\delta}^*)^{1/2} - (\hat{\delta}/\hat{\delta}^*)], \quad \text{for} \quad \hat{\delta} \le \hat{\delta}_c e^{-f\pi} \tag{24a}$$

$$\sigma_c = \sigma_o\{g(\Phi_c)[2(\hat{\delta}/\hat{\delta}^*)^{1/2} - (\hat{\delta}/\hat{\delta}^*)] + a(-f)\hat{L}_c^2\},$$

$$\text{for} \quad \hat{\delta}_c e^{-f\pi} \le \hat{\delta} \le \hat{\delta}_c \tag{24b}$$

Fig. 4 shows the prepeak σ_c-δ curve for composites with three different fiber lengths (6 mm, 8 mm, and 12 mm), in which the micromechanical parameters are close to those of steel fiber-reinforced cement. In this case the minimum critical fiber length ($L_r = 2L_c e^{-f\pi/2}$) is equal to 3 mm and the critical fiber length ($2L_c$) is equal to 10.7 mm. This means that fiber rupture (in addition to fiber pullout) will occur in any composite where the fiber length is greater than 3 mm. However, if the fiber length is less than 10.7 mm [case of Fig. 3(b)], fiber rupture will be limited to those fibers with a high inclination angle (e.g., fibers at 0° will not rupture). When the fiber length is greater than 10.7 mm [case of Fig. 3(c)], fiber rupture can occur for any fiber orientation provided that the embedment length is greater than 5.35 mm (L_c). With this in mind, it is expected that Fig. 4 should reflect an increase in the proportion of ruptured fibers as the fiber length increases from 6 to 12 mm. Fig. 4 shows that the peak composite bridging stress σ_{cu} occurs well before the fiber-rupture process is completed. It can also be seen that σ_{cu} increases with increasing fiber length. However, as the fiber length increases, the composite bridging stress decreases more rapidly thereafter, due to an increase in the proportion of ruptured fibers.

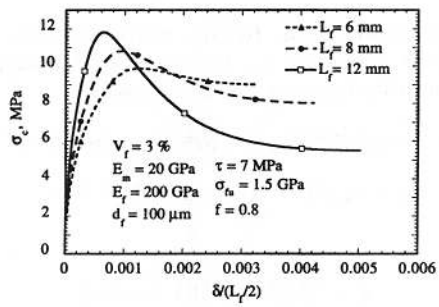

FIG. 4. Prepeak σ_c-δ Curve for Different Fiber Lengths

Postpeak Composite Bridging Stress-Displacement Relationship

The postpeak composite bridging stress-displacement relationship defines the portion of the σ_c-δ curve corresponding to the pullout stage of all surviving fibers in the composite.

$$L_r \le L_f \le 2L_c$$

Using (3*b*) in (18), (25) is obtained (Appendix II)

$$\sigma_c = \sigma_o[g(\Phi_b)(1 - \hat{\delta})^2 + b(-f)\hat{L}_c^2 - 2b(0)\hat{L}_c\hat{\delta} + b(f)\hat{\delta}^2],$$

$$\text{for} \quad \hat{\delta}^* \le \hat{\delta} \le \hat{L}_c e^{-f\pi/2} \tag{25a}$$

$$\sigma_c = \sigma_o[g(\Phi_b)(1 - \hat{\delta})^2 + c(-f)\hat{L}_c^2 - 2c(0)\hat{L}_c\hat{\delta} + c(f)\hat{\delta}^2],$$

$$\text{for} \quad \hat{L}_c e^{-f\pi/2} \le \hat{\delta} \le 1 \tag{25b}$$

where

$$b(t) = [1/(4 + t^2)]\{[2\cos(2\Phi_b) - t\sin(2\Phi_b)]e^{t\Phi_b} + 2e^{t\pi/2}\} \tag{26}$$

$$c(t) = [1/(4 + t^2)]\{[t\sin(2\Phi_a) - 2\cos(2\Phi_a)]e^{t\Phi_a} + [2\cos(2\Phi_b) - t\sin(2\Phi_b)]e^{t\Phi_b}\} \tag{27}$$

$$\Phi_a = -(1/f)\ln(\hat{\delta}/\hat{L}_c) \tag{28}$$

The angle Φ_a defines the group of fibers (fibers having an orientation satisfying $\Phi_a \le \Phi \le \pi/2$) that have already pulled out of the matrix at the COD δ.

$$L_f \ge 2L_c$$

In this case (Appendix II)

$$\sigma_c = \sigma_o[g_1\hat{L}_c^2 - 2\hat{L}_c\hat{\delta} + g\hat{\delta}^2], \quad \text{for} \quad \hat{\delta}_c \le \hat{\delta} \le \hat{L}_c e^{-f\pi/2} \tag{29a}$$

$$\sigma_c = \sigma_o[d(-f)\hat{L}_c^2 - 2d(0)\hat{L}_c\hat{\delta} + d(f)\hat{\delta}^2]$$

$$\text{for} \quad \hat{L}_c e^{-f\pi/2} \le \hat{\delta} \le \hat{L}_c \tag{29b}$$

where

$$d(t) = [1/(4 + t^2)]\{[t\sin(2\Phi_a) - 2\cos(2\Phi_a)]e^{t\Phi_a} + 2\} \tag{30}$$

$$g_1 = [2/(4 + f^2)][1 + e^{-f\pi/2}] \tag{31}$$

Note that the maximum COD is equal to L_c, the critical embedment length for fibers oriented in a direction normal to the matrix-crack plane ($\Phi = 0$).

Fig. 5 shows the postpeak σ_c-δ curve for the same composites as in Fig. 4. This figure shows that the postpeak tensile strength σ_{pp} (equal to $\sigma_c[\delta^*]$ or $\sigma_c[\delta_c]$ as appropriate) decreases with increasing fiber length due to the increase in the number of ruptured fibers. Note that the composite bridging stress vanishes at a COD equal to L_c (5.35 mm) that is less than $L_f/2$ (6 mm) for the composite with the 12-mm fibers.

Experimental Validation

The material selected for the experimental validation is a cement reinforced with 2% by volume of Kevlar 49 fibers. The dimensions and mechanical properties of the fiber used for reinforcement are given in Table 1. The fiber/matrix interfacial bond strength was measured to be 4.5 MPa by Wang

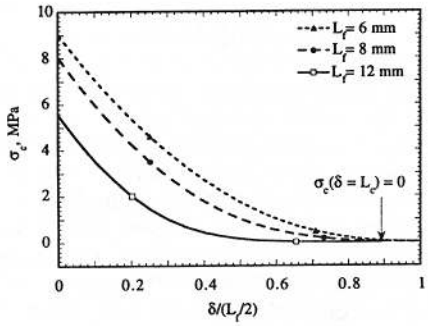

FIG. 5. Postpeak σ_c-δ Curve for Different Fiber Lengths

TABLE 1. Dimensions and Mechanical Properties of Fibers

E_f (GPa) (1)	σ_{fu} (MPa) (2)	τ (MPa) (3)	d_f (μm) (4)	L_f (mm) (5)	f (6)	Fiber density (g/cm^3) (7)
69.8[a]	3310[a]	4.5[b]	12	12.7	0.6[b]	1.44

[a]Source is Wang (1989).
[b]Assumed.

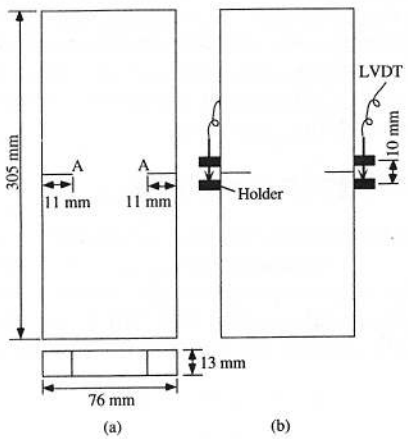

FIG. 6. Uniaxial Tension Specimen Geometry and Dimensions

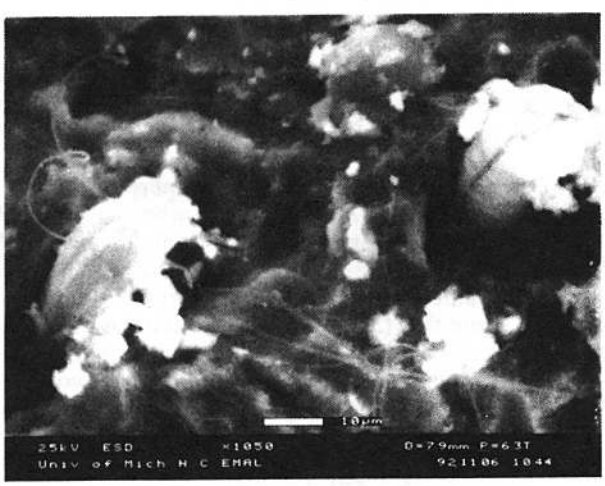

FIG. 7. SEM of Ruptured Fibers on Fracture Surface

(1989) using single fibers pullout test. The constituent materials of the matrix and their mix proportions are as follows: type I portland cement, 1.00; silica fume, 0.10; and superplasticizer, 0.02. These were used to form a cement paste with water/cementitious ratio of 0.27. The measured elastic modulus of the matrix was 13 GPa.

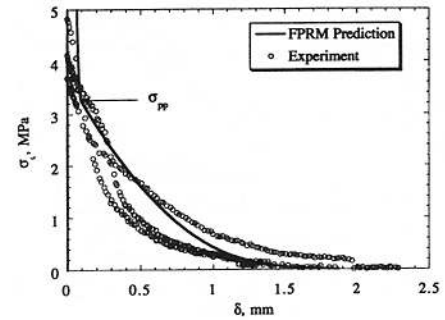

FIG. 8. Comparison between Experimentally Measured and Model Predicted σ_c-δ Curve

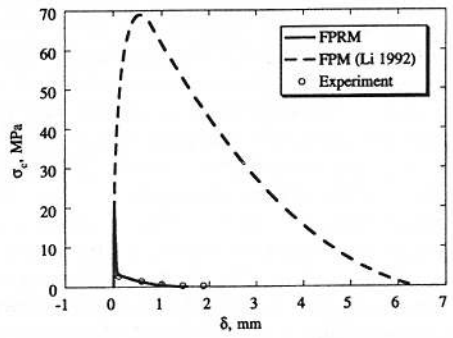

FIG. 9. Comparison between Prediction of FPM and FPRM for σ_c-δ Curve

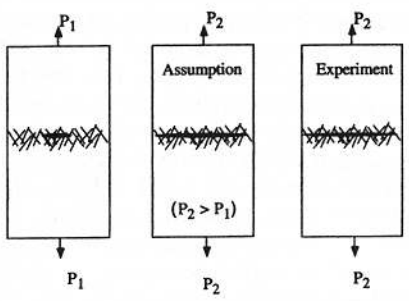

FIG. 10. Fiber Rupture and Crack Propagation

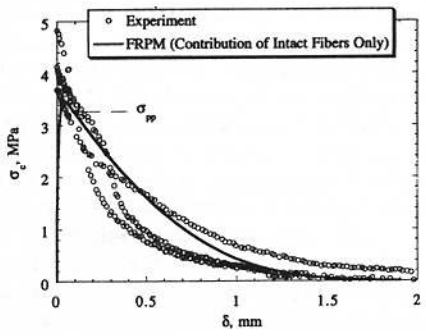

FIG. 11. Comparison between Experimentally Measured and Model Predicted σ_c-δ Curve when Contribution of Rupturing Fibers Is not Accounted for

The test is conducted on rectangular uniaxial tension specimens with a cross section of 76 × 13 mm. The specimens were cast in Plexiglas molds using high-frequency (150 Hz) vibration to improve the packing of the material and reduce air entrapment. After casting they were allowed to harden at room temperature for one day prior to demolding and then cured in water for five weeks before testing. Two notches were introduced in each specimen [Fig. 6(a)] to define the crack plane and better monitor the COD. The COD was

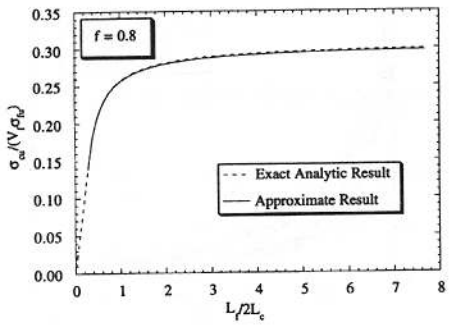

FIG. 12. Effect of Fiber Length on Composite Tensile Strength

measured using linear variable differential transducers (LVDTs). As shown in Fig. 6(b), a pair of LVDT holders were glued on side surfaces of the specimen. The relative displacement between the fixtures was measured using the two LVDTs, and the two displacement values were averaged.

Note that for this composite the fiber length is almost three times longer than the critical fiber length ($2L_c$ = 4.4 mm). This indicates that the specimens were going to fail with a large fraction of rupturing fibers. Fig. 7 shows a scanning electron microscope picture of ruptured fibers on a fracture surface of a tested specimen. The stress-COD curves obtained from three repeated uniaxial tensile tests are shown in Fig. 8 along with the prediction of the FPRM. A snubbing friction coefficient of 0.6 (within typical range [0, 1]) was used in the FPRM calculations. We can see from Fig. 8 that there is a reasonable agreement between the experimental data and the theoretical prediction for the postpeak σ_c-δ curve. Fig. 9 shows the complete σ_c-δ curve as predicted by the FPM and the FPRM. We can see from this figure that the FPM and the FPRM predict a composite tensile strength of 70 MPa and 21 MPa, respectively. However, we have measured an average postcracking strength of only 4.2 MPa.

Wang (1989) studied the chemical stability of different fibers in a cement matrix. According to Wang, Kevlar fibers are sensitive to the alkaline environment of the cement matrix and show a drop in strength after aging. In particular, after 66 days of aging in a cement matrix at 22°C and 100% relative humidity, Kevlar 49 fibers showed a 34% drop in their average strength. Because our specimens were tested at an age of 35 days, it is uncertain whether or not the Kevlar fibers have lost part of their strength. If the values of the fiber strength and bond strength are correct (leading to $L_c = \sigma_{fu} d_f / 4\tau$ = 2.2 mm), then we do not expect to see from the experiment any pullout length greater than 2.2 mm. This was found to be the case from the experimental data (Fig. 8), which shows that the composite bridging stress vanishes at an average COD of about 2.2 mm. The tension-softening behavior observed in Fig. 8 is made possible by the pullout behavior of only the surviving fibers (fibers with an embedment length less than $L_c e^{-f\Phi}$). Eye examinations of the specimen fracture surface showed protruded fibers with a maximum protrusion length around 2 mm. This confirms the validity of the fiber strength σ_{fu} and the interfacial bond strength τ used in the FPRM calculations. Therefore, the discrepancy between the measured postcracking strength and the one predicted by the FPRM may not be related to a reduction in the tensile strength of the fibers.

We should note that any prediction given by the proposed model is only valid after a crack has completely formed across a specimen. In addition, all bridging fibers are assumed intact before any loading is applied to the fibers. Therefore, the discrepancy between the measured postcracking strength (4.2 MPa) and that predicted by the model (21 MPa) could be related to the model assumption that the fibers will only start rupturing after a crack has completely formed across the specimen [along A–A in Fig. 6(a)]. In the actual test, however, the fibers were probably rupturing as the crack was propagating across the specimen section (Fig. 10). Therefore, after the crack had completely formed across the specimen, the surviving fibers become the principle contributors to the composite bridging stress. In addition, we know that if we do not account for the contribution of the rupturing fibers when computing the composite bridging stress, we expect to obtain a lower bound value for the postcracking strength. Fig. 11, which shows a comparison between the experimentally measured and the model-predicted σ_c-δ curve when the contribution of the rupturing fibers is not accounted for, indicates that this is indeed the case. In Appendix III we derive an expression for the contribution of rupturing fibers, which is subtracted from the prepeak composite bridging stress to obtain the initial part ($\delta \leq \delta_c$) of the full-line curve shown in Fig. 11. The postpeak part is the same as the one shown in Fig. 8. Fig. 11 shows also that the predicted postcracking strength (3.5 MPa) is fairly close to that experimentally measured (4.2 MPa). This evidence seems to support the explanation for the discrepancy between the postcracking strength predicted by the FPRM (21 MPa) and that experimentally measured (4.2 MPa).

For a given fiber tensile strength and interfacial bond strength, the magnitude of the postpeak tensile strength σ_{pp} depends on the assumed snubbing friction coefficient. In the absence of an independently determined value, an assumed snubbing friction coefficient of 0.6 seems to represent well the experimental data.

COMPOSITE TENSILE STRENGTH

The composite tensile strength refers to the peak composite bridging stress σ_{cu}. Although (21) and (24) cannot be solved analytically for the composite tensile strength, it is possible to obtain a numerical solution that can be accurately (error <1%) approximated by the following normalized equation:

$$\hat{\sigma}_{cu} = m_1[m_2 - \tilde{L}_f^{-1}] \tag{32}$$

where

$$\hat{\sigma}_{cu} = \sigma_{cu}/V_f\sigma_{fu} \tag{33}$$

$$m_1 = (1/125) + (19/80)e^{-(9/4)f} \tag{34}$$

$$m_2 = (g/4m_1)e^{-f(\pi/2)} + e^{f(\pi/2)} \tag{35}$$

$$\tilde{L}_f = L_f/2L_c \tag{36}$$

Eq. (32) was obtained by fitting the numerical data to an equation of the form $y = m_1(m_2 - x^{-1})$, where $x = L_f/(2L_c)$ and m_1 and m_2 = constants. This was done for every value of f in the set {0.1, 0.2, 0.3, 0.4, 0.5, 0.6, 0.7, 0.8, 0.9, 1.0}. Then the m_1 values were fitted to a function of the form $y = a + be^{cf}$. Note that (32) is only valid when the fiber length is greater than L_r. For the case when L_f is less than L_r, (19*a*) evaluated at δ^* gives the following equation for the composite tensile strength:

$$\hat{\sigma}_{cu} = (g/4)\tilde{L}_f \tag{37}$$

The m_2 equation was obtained by equating (32) and (37) at the limit value $L_f = L_r$ (i.e., $x = e^{-f\pi/2}$).

The dotted line in Fig. 12 shows the variation of normalized composite tensile strength as a function of normalized fiber length as given by (37) and the numerical solution for σ_{cu}, for a snubbing coefficient of 0.8. The solid line shows the $\hat{\sigma}_{cu} - \tilde{L}_f$ curve as given by (32). It can be seen from Fig. 12 that (32) gives a very good approximation for the composite tensile

strength. This is also the case for other snubbing coefficients in the range of 0–1 (not shown in this paper).

COMPOSITE FRACTURE ENERGY

The composite bridging fracture energy G_c can be computed in two alternative ways: either by integrating the area under the σ_c-δ curve (Li 1992), or by summing the energy contributions of the individual fibers that bridge the matrix crack plane (Li et al. 1991). Due to the complexity of integration, the first alternative does not yield an analytic solution for G_c. Therefore, the second alternative will be used.

Li et al. (1991) showed that the composite bridging fracture energy can be computed by the use of the following equation:

$$G_c = (V_f/A_f)\int_0^{L_f/2}\int_0^{\cos^{-1}(2z/L_f)} G_s(l, f, d_f, \Phi) \cdot U\{z - [(L_f/2) - L_c e^{-f\Phi}]\cos\Phi\}p(\Phi)p(z)\, d\Phi\, dz \quad (38)$$

where $G_s(l, f, d_f, \Phi)$, the energy absorption for a single fiber of embedment length l pulled out at an angle Φ, is given by the following:

$$G_s(l, f, d_f, \Phi) = (\pi/2)d_f\tau l^2 e^{f\Phi} \quad (39)$$

As written, (38) cannot be evaluated analytically. However, based on the same idea leading to (38), the composite bridging fracture energy can be computed analytically by the use of the following equation:

$$G_c = (V_f/A_f)\int_0^{\pi/2}\int_0^{(L_f/2)\cos\Phi} G_s(l, f, d_f, \Phi) \cdot U[L_c e^{-f\Phi} - l]p(z)p(\Phi)\, dz\, d\Phi \quad (40)$$

by making the change of variable $x = (2/L_f)(L_f/2 - z/\cos\Phi)$ for z, (40) becomes

$$G_c = G_o\tilde{L}_f^2\int_0^{\pi/2}\int_0^1 x^2 e^{f\Phi}U(x)\sin 2\Phi\, dx\, d\Phi \quad (41)$$

where

$$G_o = V_f\tau L_c^2/d_f \quad (42)$$

$$U(x) = 1, \quad \text{for} \quad x \le \hat{L}_c e^{-f\Phi} \quad (43a)$$

$$U(x) = 0, \quad \text{for} \quad x > \hat{L}_c e^{-f\Phi} \quad (43b)$$

Integration of (41) yields the following analytic solution for the composite fracture energy (Appendix IV):

$$\hat{G}_c = (1/3)g\tilde{L}_f^2, \quad \text{for} \quad L_f < L_r \quad (44a)$$

$$\hat{G}_c = (1/3)[g(\Phi_b)\tilde{L}_f^2 + h(\Phi_b)\tilde{L}_f^{-1}], \quad \text{for} \quad L_r \le L_f < 2L_c \quad (44b)$$

$$\hat{G}_c = (1/3)g_2\tilde{L}_f^{-1}, \quad \text{for} \quad L_f \ge 2L_c \quad (44c)$$

where

$$\hat{G}_c = G_c/G_o \quad (45)$$

$$h(\Phi_b) = [1/2(1 + f^2)][(f\sin 2\Phi_b + \cos 2\Phi_b)e^{-2f\Phi_b} + e^{-f\pi}] \quad (46)$$

$$g_2 = [1/2(1 + f^2)][1 + e^{-f\pi}] \quad (47)$$

Note that the energy absorbed by the bridging fibers during debonding is negligibly small and was not accounted for in (44).

PARAMETRIC STUDY

The purpose of the parametric study is to evaluate the effect of each micromechanical parameter (fiber length, fiber diameter, fiber strength, bond strength, and snubbing coefficient) on the composite tensile strength and fracture energy. Fig. 13 shows the effect of the fiber length on the composite tensile strength and fracture energy. This figure indicates that the composite tensile strength keeps increasing with increasing fiber length; however, the fracture energy increases initially as a function of fiber length, reaches a maximum value, and then starts to decrease. Therefore, there exists an optimum combination of tensile strength and fracture energy. This combination occurs at an optimum fiber length about $1.4L_c$ (for a snubbing coefficient of 0.8), beyond which an increase in the fiber length slightly increases the tensile strength but significantly reduces the fracture energy. When the snubbing coefficient f is zero, the optimum fiber length would be equal to $2L_c$. As the snubbing friction coefficient increases, the optimum fiber length decreases from $2L_c$ toward L_r.

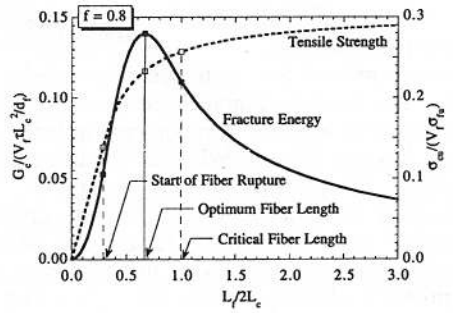

FIG. 13. Effect of Fiber Length on Composite Tensile Strength and Fracture Energy

TABLE 2. Summary of Parametric Study for Optimum σ_{cu} and G_c

Parameter (1)	Peak stress (2)	Fracture energy (3)
Fiber diameter: d_f ↑	σ_{cu} unaffected	G_c ↑
Bond strength: τ ↑	σ_{cu} unaffected	G_c ↓
Fiber strength: σ_{fu} ↑	σ_{cu} ↑	G_c ↑
Snubbing friction: f ↑	σ_{cu} ↓	G_c ↓

Table 2 summarizes the results of the parametric study. In this table, σ_{cu} and G_c refer to the composite tensile strength and fracture energy corresponding to the optimum fiber length. The table shows, in particular, that the composite tensile strength at the optimum fiber length is unaffected when the fiber diameter or the bond strength are changed. To verify this point, consider the following example: Fig. 13, a normalized curve that only depends on f, indicates that for f equal to 0.8 the normalized optimum fiber length is equal to approximately 0.7 (or $L_f = 1.4L_c = 0.35\sigma_{fu}d_f/\tau$), and the normalized tensile strength is approximately equal to 0.23 (or $\sigma_{cu} = 0.23V_f\sigma_{fu}$). When the bond strength is doubled, the optimum fiber length is reduced by 50%, but the normalized fiber length remains unchanged and so does σ_{cu}. This could also be seen from (32). Because $L_f/(2L_c)$ remains equal to 0.7, $\sigma_{cu}/(V_f\sigma_{fu})$ remains equal to 0.23. Physically, this is also reasonable. Increasing the bond strength and reducing the fiber length will result in two competing effects. The first tends to increase the strength, and the second tends to decrease it. In addition, Table 2 shows that the composite fracture energy can be enhanced by increasing the fiber diameter and/or decreasing the bond strength. In either case, the optimum fiber length will be increased. However, if the optimum fiber length is to be used in a composite, material processing can become laborious as longer fibers are generally more difficult to process. Furthermore, Table 2 shows that the tensile strength and fracture energy can both be increased by reducing the snubbing effect and/or increasing the fiber strength. In the latter case, the optimum fiber length will also

be increased. Fig. 13 and Table 2 can be used to design DRFRC for optimum performance.

For any conventional fiber-reinforced composite, it is possible to alter the micromechanical parameters such that the composite can show a better performance in terms of tensile strength and fracture energy. Whether the composite can be made to achieve its optimum properties depends on the feasible range of the micromechanical parameters, given the state of technology. For instance, fiber length can be easily customized and controlled. However, material processing can become a problem when long fibers are required for optimum performance. Furthermore, the fiber/matrix interfacial bond strength can be adjusted through, for instance, surface modification and/or mechanical crimping (Wang et al. 1991).

For any fiber/matrix system, Fig. 13 suggests that the fiber length should be neither greater than the critical fiber length $2L_c$ nor less than the minimum critical fiber length L_r for an efficient composite. Therefore, it can be concluded that the Kevlar composite, for which the fiber length is greater than $5L_c$, is not efficient. The properties of this composite can be further improved by decreasing the fiber length. This can be understood by looking at the example shown in Fig. 5. There, it is shown that by decreasing the fiber length from 12 mm to 8 mm, the postpeak tensile strength (σ_{pp}) and the fracture energy (area under the σ_c-δ curve) increased. This is due to the reduction in the fraction of ruptured fibers. Furthermore, decreasing the fiber length is particularly useful for the Kevlar fiber composite as the rupturing fibers do not seem to significantly contribute to postcracking strength. Alternatively, the composite properties can be improved by one or a combination of the following: (1) increase the fiber tensile strength; (2) increase the fiber diameter; (3) reduce the bond strength; and (4) reduce the snubbing coefficient. All of these alternatives amount to increasing the optimum fiber length. If these alternatives are possible, the used fiber length of 12 mm will become at some point the optimum fiber length.

CONCLUSIONS

In this paper, a micromechanical model for the composite bridging stress-COD relationship that accounts for fiber pullout and tensile rupture was presented. The model accounts for a local frictional effect called snubbing; however, it does not account for fiber-bending rupture and the possible effect of matrix spalling at the exit points of inclined fibers from the matrix. The model assumes a fiber/matrix interface that is controlled by a constant frictional bond stress. The postpeak σ_c-δ curve predicted by the new model is in good agreement with the one measured for a Kevlar fiber-reinforced cement in which fiber rupture has occurred. The model yielded analytical expressions for the composite tensile strength and fracture energy and produced a tool for designing DRFRC for optimum performance. Using this model, the behavior of the composite can be controlled through the microstructural properties. Therefore, the composite can be designed to achieve (1) the highest fracture energy; (2) the highest tensile strength; (3) the highest flexural strength (as this can be related to the σ_c-δ relationship); and (4) a compromise between the preceding three properties that fits a particular engineering application. However, there are practical and theoretical limitations to this model. First, fibers are generally supplied at discrete sizes. Second, the processing technique might restrict the fiber length to a certain maximum limit so that fibers with optimum length become difficult if not impossible to handle. Third, this model is more applicable to fibers having a high Weibull modulus, m (e.g., for steel fibers $m \approx 100$). Fibers with a low Weibull modulus (e.g., for carbon fibers $m \approx 10$) will not necessarily rupture at the matrix-crack plane. For these fibers, therefore, the strength distribution should be accounted for in the model. If the fibers are brittle, bending rupture will also need to be included in a composite model.

ACKNOWLEDGMENTS

The work reported in this paper has been partially supported by grant BCS-9202097 from the National Science Foundation and grant SHRP-91-ID036 030219 from the National Research Council to the University of Michigan. A U-M Rackham Predoctoral Fellowship Award supported the PhD study of M. Maalej. T. Hashida was a visiting research fellow at the University of Michigan in 1991–1993.

APPENDIX I. DERIVATION OF PREPEAK σ_c-δ RELATIONSHIP

$L_r \le L_f \le 2L_c$

The prepeak composite bridging stress is composed of three contributions from individual fibers. For those fibers having an embedment length l greater than $L_c e^{-f\Phi}$, their contribution is through fiber debonding. Each one of these fibers starts debonding as the load is applied and eventually breaks at a COD equal to $\delta_c e^{-2f\Phi}$. After rupture, the contribution of that fiber to σ_c is discounted. For the second group of fibers, their contribution is also through fiber debonding. Fibers in the second group pass into a third group as δ increases. The contribution of the fibers in the third group is through fiber pullout.

For the first group: $l \ge l_u \Rightarrow x \ge \hat{l}_u$. Because the first group contains only those fibers that eventually rupture, it is necessary that $\Phi \ge \Phi_b$. Using (12) in (18), (48) is obtained as follows:

$$\sigma_{c1} = (V_f/2) \int_{\Phi_b}^{\pi/2} \int_{\hat{l}_u}^{1} \sigma_d U(\delta_c e^{-2f\Phi} - \delta) e^{f\Phi} \sin 2\Phi \, dx \, d\Phi \tag{48}$$

substituting $U(\delta_c e^{-2f\Phi} - \delta)$ in (48), the following equation is obtained:

$$\sigma_{c1} = (V_f/2) \int_{\Phi_b}^{\Phi_c} \int_{\hat{l}_u}^{1} \sigma_d e^{f\Phi} \sin 2\Phi \, dx \, d\Phi \tag{49}$$

Contribution of fibers of the second group is composed of the contribution of those fibers that are oriented in such a way ($0 \le \Phi \le \Phi_b$) that they do not rupture (regardless of their embedment length) as well as the other fibers that have an embedment length short enough ($l < l_u$) that they did not rupture. Fibers of the second group eventually pull out. During debonding, it is necessary that $\delta \le \delta_o \Rightarrow x \ge x_o$, where $x_o = (\hat{\delta}/\hat{\delta}^*)^{1/2}$, therefore

$$\sigma_{c2} = (V_f/2) \left\{ \int_0^{\Phi_b} \int_{x_0}^{1} \sigma_d e^{f\Phi} \sin 2\Phi \, dx \, d\Phi + \int_{\Phi_b}^{\pi/2} \int_{x_0}^{\hat{l}_u} \sigma_d e^{f\Phi} \sin 2\Phi \, dx \, d\Phi \right\} \tag{50}$$

The lower limits for x in (50) insures that only those fibers not fully debonded are counted in this contribution. The upper limit for x in the second term on the right hand side of (50) insures that only those fibers that are eventually going to pull out (rather than rupture) are accounted for in this contribution. Because $x_o \le \hat{l}_u$, (50) becomes

$$\sigma_{c2} = (V_f/2) \left\{ \int_0^{\Phi_b} \int_{x_0}^{1} \sigma_d e^{f\Phi} \sin 2\Phi \, dx \, d\Phi + \int_{\Phi_b}^{\Phi_c} \int_{x_0}^{\hat{l}_u} \sigma_d e^{f\Phi} \sin 2\Phi \, dx \, d\Phi \right\} \tag{51}$$

Fibers of the second group that have debonded pass into the third group. During pullout, $\delta \le l \Rightarrow x \ge \hat{\delta}$, thus

$$\sigma_{c3} = (V_f/2)\left\{\int_0^{\Phi_b}\int_{\hat{\delta}}^{x_0} \sigma_p e^{f\Phi} \sin 2\Phi \, dx \, d\Phi + \int_{\Phi_b}^{\pi/2}\int_{\hat{\delta}}^{x_0} \sigma_p e^{f\Phi} \sin 2\Phi \, dx \, d\Phi\right\} \quad (52)$$

The lower limits for x in (52) insures that only the fibers that have not fully pulled out are accounted for in this contribution. Using the fact the for those fibers oriented at an angle greater than Φ_b, the embedment length l should be less than the critical embedment length l_u and (52) can be rewritten as follows:

$$\sigma_{c3} = (V_f/2)\left\{\int_0^{\Phi_c}\int_{\hat{\delta}}^{x_o} \sigma_p e^{f\Phi} \sin 2\Phi \, dx \, d\Phi + \int_{\Phi_c}^{\pi/2}\int_{\hat{\delta}}^{\hat{l}_u} \sigma_p e^{f\Phi} \sin 2\Phi \, dx \, d\Phi\right\} \quad (53)$$

Combining all terms, the following equation is obtained:

$$\sigma_c = (V_f/2)\left\{\int_0^{\Phi_c}\int_{x_o}^{1} \sigma_d e^{f\Phi} \sin 2\Phi \, dx \, d\Phi + \int_0^{\Phi_c}\int_{\hat{\delta}}^{x_o} \sigma_p e^{f\Phi} \sin 2\Phi \, dx \, d\Phi + \int_{\Phi_c}^{\pi/2}\int_{\hat{\delta}}^{\hat{l}_u} \sigma_p e^{f\Phi} \sin 2\Phi \, dx \, d\Phi\right\} \quad (54)$$

For $\delta \le \delta_c e^{-f\pi}$ and $\Phi_c = \pi/2$, (54) becomes

$$\sigma_c = (V_f/2)\left\{\int_0^{\pi/2}\int_{x_o}^{1} \sigma_d e^{f\Phi} \sin 2\Phi \, dx \, d\Phi + \int_0^{\pi/2}\int_{\hat{\delta}}^{x_o} \sigma_p e^{f\Phi} \sin 2\Phi \, dx \, d\Phi\right\} \quad (55)$$

Evaluation of (55) gives

$$\sigma_c = \sigma_o g[2(\hat{\delta}/\hat{\delta}^*)^{1/2} - (\hat{\delta}/\hat{\delta}^*) - (4/3)\hat{\delta}^*(\hat{\delta}/\hat{\delta}^*)^{3/2} + \hat{\delta}^2 - (2/3)\hat{\delta}^*\hat{\delta}^3] \quad (56)$$

For $\delta_c e^{-f\pi} \le \delta \le \delta^*$, (54) gives

$$\sigma_c = \sigma_o\{g(\Phi_c)[2(\hat{\delta}/\hat{\delta}^*)^{1/2} - (\hat{\delta}/\hat{\delta}^*) - (4/3)\hat{\delta}^*(\hat{\delta}/\hat{\delta}^*)^{3/2} + \hat{\delta}^2 - (2/3)\hat{\delta}^*\hat{\delta}^3] + a(-f)\hat{L}_c^2 - 2a(0)\hat{L}_c\hat{\delta} + a(f)[1 - (2/3)\hat{\delta}^*\hat{\delta}]\hat{\delta}^2 + (2/3)a(-2f)\hat{L}_c^3\hat{\delta}^*\} \quad (57)$$

For $\hat{\delta}^* << 1$ (which is generally the case), the prepeak σ_c-δ relationship can be reduced to the simplified form in (21).

$L_f \ge 2L_c$

In this case, the angle Φ_b is equal to zero. Therefore, fiber rupture can occur for any fiber orientation, provided the embedment length l is greater than the critical embedment length l_u. Furthermore, the fiber rupture process ends at a COD equal to δ_c rather than δ^*. Following the same analysis given earlier for Φ_b equal to zero, the same expressions for σ_c as given by (54)–(57) are obtained.

APPENDIX II. DERIVATION OF POSTPEAK σ_c-δ RELATIONSHIP

$L_r \le L_f \le 2L_c$

For $\delta \ge \delta^*$, all fibers would be slipping. However, some fibers were ruptured and they should be discounted when computing the composite bridging stress. The postpeak composite bridging stress is composed of the contribution of those fibers from the third group defined in Appendix I. The composite bridging stress may then be written as follows:

$$\sigma_c = (V_f/2)\left\{\int_0^{\Phi_b}\int_{\hat{\delta}}^{1} \sigma_p e^{f\Phi} \sin 2\Phi \, dx \, d\Phi + \int_{\Phi_b}^{\pi/2}\int_{\hat{\delta}}^{\hat{l}_u} \sigma_p e^{f\Phi} \sin 2\Phi \, dx \, d\Phi\right\} \quad (58)$$

The lower limits for x in (58) insure that only the fibers that have not fully pulled out are accounted for in this contribution. The upper limit for x in the second term on the right-hand side of (58) insures that only those fibers that did not break are counted in this contribution. Using the fact that for those fibers oriented at an angle greater than Φ_b the embedment length l should be less than the critical embedment length l_u, (58) becomes

$$\sigma_c = (V_f/2)\left\{\int_0^{\Phi_b}\int_{\hat{\delta}}^{1} \sigma_p e^{f\Phi} \sin 2\Phi \, dx \, d\Phi + \int_{\Phi_b}^{\Phi_a}\int_{\hat{\delta}}^{\hat{l}_u} \sigma_p e^{f\Phi} \sin 2\Phi \, dx \, d\Phi\right\} \quad (59)$$

For $\delta^* \le \delta \le L_c e^{-f\pi/2}$ and $\Phi_a = \pi/2$, (59) gives

$$\sigma_c = \sigma_o\{g(\Phi_b)[(1 - \hat{\delta})^2 + (2/3)\hat{\delta}^*(1 - \hat{\delta}^3)] + b(-f)\hat{L}_c^2 - 2b(0)\hat{L}_c\hat{\delta} + b(f)(1 - (2/3)\hat{\delta}^*\hat{\delta})\hat{\delta}^2 + (2/3)b(-2f)\hat{L}_c^3\hat{\delta}^*\} \quad (60)$$

For $L_c e^{-f\pi/2} \le \delta \le L_f/2$, (59) gives

$$\sigma_c = \sigma_o\{g(\Phi_b)[(1 - \hat{\delta})^2 + (2/3)\hat{\delta}^*(1 - \hat{\delta}^3)] + c(-f)\hat{L}_c^2 - 2c(0)\hat{L}_c\hat{\delta} + c(f)(1 - (2/3)\hat{\delta}^*\hat{\delta})\hat{\delta}^2 + (2/3)c(-2f)\hat{L}_c^3\hat{\delta}^*\} \quad (61)$$

For $\hat{\delta}^* << 1$, the postpeak σ_c-δ relationship can be reduced to the simplified form in (25).

$L_f \ge 2L_c$

In this case the postpeak σ_c-δ relationship can be obtained simply by substituting zero for Φ_b in (60)–(61).

For $\delta_c \le \delta \le L_c e^{-f\pi/2}$, (60) gives

$$\sigma_c = \sigma_o[g_1\hat{L}_c^2 - 2\hat{L}_c\hat{\delta} + g(1 - (2/3)\hat{\delta}^*\hat{\delta})\hat{\delta}^2 + (2/3)g_2\hat{L}_c^3\hat{\delta}^*] \quad (62)$$

For $L_c e^{-f\pi/2} \le \delta \le L_c$, (61) gives

$$\sigma_c = \sigma_o[d(-f)\hat{L}_c^2 - 2d(0)\hat{L}_c\hat{\delta} + d(f)(1 - (2/3)\hat{\delta}^*\hat{\delta})\hat{\delta}^2 + (2/3)d(-2f)\hat{L}_c^3\hat{\delta}^*] \quad (63)$$

Note that (63) vanishes at a COD equal to L_c. For $\hat{\delta}^* << 1$, the postpeak σ_c-δ relationship can be reduced to the simplified form in (29).

APPENDIX III. DERIVATION OF PREPEAK σ_c-δ RELATIONSHIP WITHOUT ACCOUNTING FOR CONTRIBUTION OF RUPTURING FIBERS

To discount the contribution of the rupturing fibers from the composite bridging stress, σ_{c1}, which was defined in (49), should be subtracted from σ_c as express in (56) for $\delta \le \delta_c e^{-f\pi}$, and (57) for $\delta_c e^{-f\pi} \le \delta \le \delta_p$ (where $\delta_p = \delta^*$ for $L_r \le L_f \le 2L_c$, and $\delta_p = \delta_c$ for $L_f \ge 2L_c$).

$L_r \le L_f \le 2L_c$

For $\delta \le \delta_c e^{-f\pi}$, $\Phi_c = \pi/2$. Evaluation of (49) gives

$$\sigma_{c1} = 2\sigma_o(\hat{\delta}/\hat{\delta}^*)^{1/2}(\{[1 + \cos(2\Phi_b)]/2\}\hat{L}_c - k(\Phi_b, \pi/2)) \quad (64)$$

where

$$k(u, v) = [1/(4 + f^2)]\{[f \sin(2u) - 2\cos(2u)]e^{fu} + [2\cos(2v) - f\sin(2v)]e^{fv}\} \quad (65)$$

For $\delta_c e^{-f\pi} \le \delta \le \delta^*$, evaluation of (49) gives

$$\sigma_{c1} = 2\sigma_o(\hat{\delta}/\hat{\delta}^*)^{1/2}(\{[\cos(2\Phi_c) - \cos(2\Phi_b)]/2\}\hat{L}_c - k(\Phi_b, \Phi_c)) \quad (66)$$

$L_f \ge 2L_c$

In this case, $\Phi_b = 0$. For $\delta \le \delta_c e^{-f\pi}$, $\Phi_c = \pi/2$. Evaluation of (49) gives

$$\sigma_{c1} = 2\sigma_o(\hat{\delta}/\hat{\delta}^*)^{1/2}[g - \hat{L}_c] \quad (67)$$

For $\delta_c e^{-f\pi} \le \delta \le \delta_c$, evaluation of (49) gives

$$\sigma_{c1} = 2\sigma_o(\hat{\delta}/\hat{\delta}^*)^{1/2}(\{[\cos(2\Phi_c) - 1]/2\}\hat{L}_c - k(0, \Phi_c)) \quad (68)$$

APPENDIX IV. DERIVATION OF COMPOSITE FRACTURE ENERGY

$L_r \le L_f \le 2L_c$

The composite bridging fracture energy is composed of the contribution of those fibers from the third group defined in Appendix I. Therefore, (41) may be written as follows:

$$G_c = G_o\tilde{L}_f^2\left[\int_0^{\Phi_b}\int_0^1 x^2 e^{f\Phi}\sin 2\Phi\, dx\, d\Phi + \int_{\Phi_b}^{\pi/2}\int_0^{\hat{l}_u} x^2 e^{f\Phi}\sin 2\Phi\, dx\, d\Phi\right] \quad (69)$$

The upper limit for x in the second term on the right-hand side of (69) insures that only those fibers that did not break are counted in this contribution. Evaluation of (69) yields (44*b*).

$L_f \le L_r$

In this case the composite bridging fracture energy can be computed by substituting $\pi/2$ for Φ_b in (69)

$$G_c = G_o\tilde{L}_f^2\int_0^{\pi/2}\int_0^1 x^2 e^{f\Phi}\sin 2\Phi\, dx\, d\Phi \quad (70)$$

Evaluation of (70) yields (44*a*).

$L_f \ge 2L_c$

In this case the composite bridging fracture energy can be computed by substituting zero for Φ_b in (69)

$$G_c = G_o\tilde{L}_f^2\int_0^{\pi/2}\int_0^{\hat{l}_u} x^2 e^{f\Phi}\sin 2\Phi\, dx\, d\Phi \quad (71)$$

Evaluation of (71) yields (44*c*).

APPENDIX V. REFERENCES

Krenchel, H., and Hansen, S. (1992). "New recipes and new production techniques for high performance FRC-materials." *Proc., Int. Workshop on High Perf. Fiber Reinforced Cement Composites*, H. Reinhardt and A. Naaman, eds., Chapman & Hall, Ltd., London, England, 65–83.

Li, V. C. (1992). "Postcrack scaling relations for fiber reinforced cementitious composites." *J. Mat. in Civ. Engrg.*, ASCE, 4(1), 41–57.

Li, V. C., and Chan, Y. W. (1994). "Determination of interfacial debond mode for fiber reinforced cementitious composites." *J. Engrg. Mech.*, ASCE, 120(4), 707–719.

Li, V. C., and Leung, K. Y. (1992). "Steady state and multiple cracking of short random fiber composites." *J. Engrg. Mech.*, ASCE, 118(11), 2246–2264.

Li, V. C., and Wu, H. C. (1992). "Pseudo strain-hardening design in cementitious composites." *Proc., Int. Workshop on High Perf. Fiber Reinforced Cement Composites*, H. Reinhardt and A. Naaman, eds., Chapman & Hall, Ltd., London, England, 371–387.

Li, V. C., Chan, C. M., and Leung, C. K. Y. (1987). "Experimental determination of the tension softening relations for cementitious composites." *Cement and Concrete Res.*, 17(3), 441–452.

Li, V. C., Wang, Y., and Backer, S. (1990). "Effect of inclining angle, bundling, and surface treatment on synthetic fiber pull-out from a cement matrix." *J. Composites*, 21(2), 132–140.

Li, V. C., Wang, Y., and Backer, S. (1991). "A micromechanical model of tension softening and bridging toughening of short random fiber reinforced brittle matrix composites." *J. Mech. Phys. Solids*, 39(5), 607–625.

Visalvanich, K., and Naaman, A. E. (1983). "Fracture model for fiber reinforced concrete." *ACI J.*, 80(2), 128–138.

Wang, Y. (1989). "Mechanics of fiber cementitious composites," PhD thesis, Massachusetts Inst. of Technol., Cambridge, Mass.

Wang, Y., Li, V. C., and Backer, S. (1991). "Tensile failure mechanisms in synthetic fiber-reinforced mortar." *J. Mat. Sci.*, 26(24), 6565–6575.

APPENDIX VI. NOTATION

The following symbols are used in this paper:

d_f = fiber diameter;
E_f = fiber-elastic modulus;
E_m = matrix-elastic modulus;
f = snubbing friction coefficient;
G_c = composite fracture energy;
L_c = critical embedment length for fiber inclined at $\Phi = 0$;
$2L_c$ = critical fiber length;
L_f = fiber length;
L_r = minimum critical fiber length;
l = fiber embedment length;
l_u = critical embedment length;
$p(\Phi)$ = probability density function of fiber inclination angle;
$p(z)$ = probability density function of fiber centroidal distance;
S = fiber rupture space;
$S_{\Phi b}$ = fiber rupture space when $L_r \le L_f \le 2L_c$;
t = dummy variable that takes the values of $-2f$, $-f$, 0, and f;
V_f = fiber volume fraction;
z = fiber centroidal location;
δ = crack opening displacement (COD);
δ^* = COD at which frictional debonding reaches end of longest embedment length $l = L_f/2$;
δ_c = critical COD for fiber inclined at $\Phi = 0$;
δ_o = COD at which frictional debonding reaches end of embedment length l;
δ_u = critical COD;

σ_b = fiber bridging stress;
σ_c = composite bridging stress;
σ_{cu} = composite tensile strength;
σ_d = fiber debonding stress;
σ_{fu} = fiber tensile strength;
σ_p = fiber pullout stress;
σ_{pp} = postpeak tensile strength: $\sigma_c[\delta^*]$ or $\sigma_c[\delta_c]$ as appropriate;
τ = interfacial frictional bond strength; and
Φ = fiber inclination angle with respect to direction normal to matrix crack plane.